THE ASTROPHYSICAL JOURNAL, 342:759–768, 1989 July 15

FAR-INFRARED EMISSION AND STAR FORMATION IN SPIRAL GALAXIES

G. TRINCHIERI,[1,2] G. FABBIANO,[2] AND R. BANDIERA[1]
Received 1987 December 28; accepted 1988 December 29

ABSTRACT

We present a statistical study of a sample of normal spiral galaxies, which investigates the correlations between the emission in the far-infrared, Hα and blue, together with a comprehensive comparison of other related quantities (optical and infrared colors, and the Hα equivalent width). This study is different from previous ones because it takes into account several different quantities *at the same time* and can therefore investigate whether correlations among different quantities are directly related to a given astrophysical phenomenon, or are a by-product of more hidden fundamental relations, or merely result from the sampling of galaxies with a large range in size, mass, and luminosity.

We find that the luminosities in these three bands are all tightly correlated, although both the strength of the correlations and their functional dependencies are a function of the galaxies' morphological types. The best-fit power laws to these correlations are different for the comparison of different quantities and deviate significantly from linearity in some cases, implying the presence of additional emission mechanisms not related to the general increase of luminosity with galactic mass.

We find clear evidence of two independent affects in the incidence of the warm far-infrared emission in late-type spirals. One is a luminosity effect, as shown by the presence of excess far-infrared relative to their Hα or optical emission in the more luminous galaxies, coupled with warmer far-infrared colors. This evidence is interpreted in terms of a warm far-infrared component, produced in highly obscured stardust regions, and present only in high-luminosity objects. The second effect is a dependence on widespread star-formation activity, measured by larger Hα equivalent widths. The present results can be used to set some constraints on the mass function of disk galaxies and indicate that if there is a break (alternatively, if the mass function is bimodal), the change should occur at masses lower than $M \sim 1$–$2\ M_{\odot}$.

Subject headings: galaxies: interstellar matter — galaxies: photometry — stars: formation

I. INTRODUCTION

A considerable part of the stellar energy output of normal spiral galaxies is reemitted in the far-infrared as thermal emission of interstellar dust. Following the *IRAS* all sky survey, much effort has been spent in investigating the properties of this radiation, to understand how well it traces star formation, and to use it as an indicator of the stellar composition of spiral galaxies. The picture that emerges from these studies is not unique. While the correlation of the far-infrared emission with Hα has reinforced a close connection between far-infrared and star formation (Moorwood, Veron-Cetty, and Glass 1987), other work suggested the presence of at least two emission components, the cooler of which could be associated with the general stellar field (e.g., Persson and Helou 1987, hereafter PH; see also Cox, Krueger, and Mezger 1986). The occurrence of the warmer component, linked to recent star formation, is also controversial. While PH associate this component with bluer star-forming galaxies, Fabbiano, Gioia, and Trinchieri (1988, hereafter FGT; see also de Jong 1986; Helou 1987) suggest that this component is instead found preferentially in more luminous/massive galaxies, which typically do not have bluer optical colors.

The aim of this paper is to investigate further these issues, by comparing the integrated properties of the emission in the far-infrared, optical continuum (*B*), and Hα in spiral galaxies in a comprehensive statistical manner. In this work we pay attention not only to the presence of correlations, but to their functional dependence. Deviations from linear proportionality could indicate the presence of some additional emission mechanism, rather than a general increase of luminosity linked to a single galaxy parameter (e.g., mass). Moreover, we give quantitative estimates of the significance of the observed correlations in the attempt to discriminate between the secondary effects of strongest correlations and the driving correlations themselves, that should be examined in the light of different model predictions.

This work is the natural extension of that presented in FGT, where the statistical properties of normal galaxies were investigated by studying correlations among five different observational wavebands (radio, near- and far-infrared, optical, and X-rays). The present sample is different from those used by FGT, because Hα fluxes are not available for most of those galaxies. However, in both cases, the samples can be considered representative of spiral galaxies, and our results can be complemented by those of FGT. The sample used in this work overlaps considerably with that used by PH, and we perform a statistical analysis of the emission in the same three wavebands used by these authors. However, the use of different more quantitative techniques, and the availability of related work encompassing different indicators (e.g., FGT), lead us to different conclusions.

II. SAMPLE SELECTION

In this analysis we use a subsample of the 175 normal galaxies observed by Kennicutt and Kent (1983) in the Hα line. The original sample was selected from the Shapley-Ames (Sandage and Tamman 1981) catalog, mostly for galaxies with *UBV* photometry. Although the resulting sample undersamples intrinsically faint galaxies, it should be a fair represen-

[1] Osservatorio Astrofisico di Arcetri, Firenze.
[2] Harvard Smithsonian Center for Astrophysics.

TABLE 1

THE SAMPLE

Galaxy NGC	T	Distance (Mpc)	$\log l_B$ (ergs s^{-1} Hz^{-1})	$\log L_{H\alpha}$ (ergs s^{-1})	$\log L_{FIR}$ (ergs s^{-1})	Galaxy NGC	T	Distance (Mpc)	$\log l_B$ (ergs s^{-1} Hz^{-1})	$\log L_{H\alpha}$ (ergs s^{-1})	$\log L_{FIR}$ (ergs s^{-1})
150	3	32.4	29.05	41.45	43.83	4571	7	20.5	28.62	40.68	42.75
157	4	36.3	29.58	41.86	44.15	4595	3	20.5	28.11	40.2	42.53
278	3	18.6	28.88	41.44	43.74	4597	9	17	28.03	40.7	42.27
337	7	35.5	29.12	41.65	43.86	4602	4	46.9	29.11	41.39	43.94
428	9	26.1	28.94	41.06	42.96	4631	7	12.1	29.29	41.53	43.97*
450	6	38.2	29.00	41.36	43.40	4632	5	31.1	28.88	41.36	43.49
628	5	17.2	29.41	41.67	43.73*	4651	5	20.5	28.95	41.21	43.26
672	6	12.9	28.65	40.74	42.63	4654	6	20.5	29.05	41.2	43.64
949	3	17.1	28.42	40.72	42.90	4658	4	44	29.06	41.21	43.75
1022	1	31.5	28.99	40.93	44.08	4666	5	29.5	29.28	41.73	44.28
1058	6	14.8	28.41	40.54	42.71	4689	4	20.5	28.71	40.9	43.02
1073	5	26.4	29.08	41.17	42.97	4713	7	22.9	28.7	41.39	43.24
1084	5	29.6	29.38	41.83	44.20	4736	2	7.1	29.00	40.89	43.36*
1087	5	32.6	29.31	41.65	43.93	4775	7	27.5	28.97	41.27	43.34
1140	10	31.2	28.78	41.36	43.27	4781	7	13.8	28.33	40.71	43.04
1156	10	11.2	28.14	40.53	42.66	4790	5	23.1	28.46	40.83	43.01
1232	5	35.5	29.74	42.00	43.67	4808	6	12.6	27.93	40.61	42.43
1385	6	39.4	29.41	41.89	44.25	4826	2	7	28.83	40.42	43.09*
1518	8	18.3	28.54	40.83	42.78	4900	5	16.5	28.41	40.99	43.03
1569	10	2.9	27.42	40.37	42.34	4941	2	17.6	28.63	40.64	42.54
1637	5	14.3	28.6	40.7	42.94	5005	4	20.8	29.29	41.01	43.85
1832	4	37.1	29.34	41.59	43.85	5033	5	17.9	29.17	41.28	43.67*
2139	6	33.8	29.17	41.59	43.73	5055	4	11	29.24	41.33	43.68*
2276	5	53	29.6	42.03	44.40	5194	4	10.8	29.35	41.62	43.84*
2763	6	33.2	28.86	41.21	43.27	5204	9	7.4	27.94	40.25	41.97
2976	5	4.8	27.96	39.89	42.29	5248	4	21	29.17	41.39	43.77
3185	1	23	28.4	40.1	42.78	5364	4	22.8	29.17	41.32	43.12
3310	4	21.5	29.03	41.83	43.95	5474	6	7.4	28.03	40.13	41.80
3351	3	12.8	28.87	40.95	43.29	5585	7	7.4	28.06	40.12	41.69
3368	2	15.2	29.17	40.88	43.24	5633	3	48.7	29.12	41.41	43.72
3389	5	22.5	28.65	41.00	—	5676	4	44.8	29.57	41.76	44.23
3486	5	12.7	28.71	41.09	42.80	5701	0	28.5	28.92	40.9	<42.47
3504	2	29.6	29.06	41.56	44.03	5746	3	32.8	29.53	41.54	43.25
3521	4	12.5	29.21	41.32	43.75*	5806	3	25.4	28.83	40.92	43.16
3627	3	11.9	29.17	41.28	43.80*	5962	5	39.4	29.26	41.54	44.01
3631	5	24.8	29.21	41.55	43.59	5970	5	40.9	29.27	41.83	43.61
3726	5	18.2	28.99	41.09	43.06	6015	6	20.4	28.92	41.27	43.07
3810	5	17.2	28.82	41.25	43.41	6070	6	39.6	29.25	41.47	43.77
3938	5	16.9	28.92	41.21	43.18	6106	5	29.2	28.78	41.21	43.05
3955	0	21.2	28.59	40.8	43.41	6181	5	48.8	29.35	41.84	44.19
4027	8	28.4	29.12	41.5	43.82	6207	5	19.7	28.67	41.08	43.13
4152	5	41.1	28.96	41.45	43.71	6217	4	32	29.18	41.49	43.87
4178	8	20.5	28.8	41.03	42.89	6412	5	31.4	28.97	41.15	43.27
4189	6	20.5	28.44	40.75	43.03	6503	6	6.1	28.24	40.33	42.39
4212	4	20.5	28.73	41.05	43.32	6574	4	46.3	29.28	41.6	44.32
4214	10	5.8	28.29	40.76	42.50	6643	5	34.9	29.39	41.72	44.03
4237	4	20.5	28.35	40.25	43.01	6814	4	32.9	29.31	41.5	43.72
4254	5	20.5	29.28	41.84	43.92	6946	6	6.7	28.98	41.1	43.68*
4294	6	20.5	28.51	41.04	42.90	7137	5	39	28.9	41.27	...
4298	5	20.5	28.67	40.73	43.28	7177	3	28.4	29.08	40.8	...
4299	8	20.5	28.28	41.04	42.86	7217	2	24.7	29.32	41.2	43.46
4303	4	22.9	29.46	41.9	43.99	7218	6	35.6	29.02	41.35	43.62
4321	4	20.5	29.4	41.7	43.82	7392	4	60.7	29.41	41.53	43.87
4420	4	30.3	28.69	41.22	43.28	7448	4	49.7	29.49	41.89	44.15
4449	10	5	28.32	40.88	—	7479	5	52.6	29.64	41.66	44.37
4487	6	16.6	28.37	40.64	42.68	7590	4	29.7	29.04	41.53	43.69
4496	9	22.9	28.65	41.06	43.18	7716	3	54.7	29.16	41.19	43.25
4501	3	20.5	29.4	41.25	43.76	7723	3	39.5	29.32	41.29	43.70
4504	6	15.9	28.21	40.71	42.52	7741	6	20.6	28.75	40.99	42.90
4535	5	20.5	29.21	41.32	43.38	7742	3	38	29.1	41.25	43.50
4536	4	32.9	29.56	41.63	44.30	7764	10	33.5	28.87	41.16	...
4548	3	20.5	29.06	40.7	42.84	IC 4662	10	4.8	27.77	40.3	42.06
4561	8	22.9	28.29	40.46	42.66	IC 5271	3	35.2	28.78	40.58	43.51
4569	2	20.5	29.43	41.13	43.52*						

NOTE.—Distances are from the Shapley-Ames Catalog, with $H_0 = 50$ km s^{-1} Mpc^{-1}. Optical luminosities are derived from B_T ($B_T{}^0$ when possible) as given in deVaucouleurs, de Vaucouleurs, and Corwin 1976. Hα luminosities are from Kennicutt and Kent 1983. FIR luminosities are from the *IRAS* catalog (Lonsdale *et al.* 1985), or from Rice *et al.* 1988 if marked with asterisk (*).

tation of spirals brighter than $M < -17$ (Kennicutt and Kent 1983). We have used only those 127 spiral and irregular galaxies for which integrated Hα fluxes over the whole galactic disk are available, due to lack of information on the upper limits to the Hα fluxes for the remaining galaxies. As discussed in § III this selection should not bias our results. Table 1 lists the sample galaxies together with their distances and Hα luminosities as given in Kennicutt and Kent; the morphological parameter T and the blue luminosities (from the corrected optical magnitudes B_T^0 when possible) from deVaucouleurs, de Vaucouleurs, and Corwin (1976); and the far-infrared luminosities derived from the wide band fluxes (FIR) given in the *IRAS* catalog (Cataloged Galaxies and Quasars Observed in the IRAS Survey 1985), or from Rice *et al.* (1988) for 11 galaxies with apparent isophotal diameter larger than 8′. Of the 127 galaxies, 121 are detected at both 60 and 100 μm. Five galaxies are not included in the *IRAS* catalog, and for one an upper limit is given.

For the purpose of this paper, we have divided the galaxies into two subsamples, according to their morphological classification: the "early" ($0 \leq T \leq 4$, or Sa to Sbc) and "late" ($T \geq 5$, Sc to Irr) spiral samples, of 52 and 75 objects, respectively. This subdivision distinguishes between bulge-dominated and disk-dominated systems. Galaxies with $T = 4$ have intermediate properties, and we have included them in the early-type sample to obtain a cleaner late-type sample. In what follows, we will always refer to galaxies according to this subdivision, unless specifically stated otherwise.

III. DATA ANALYSIS AND RESULTS

a) Correlation Analysis

Figure 1 shows the L_{FIR}–$L_{H\alpha}$, $L_{H\alpha}$–l_B, and L_{FIR}–l_B plots for the subsamples of early- and late-type spirals. Strong correlations exist between each pair of the quantities for both samples, and these correlations follow different slopes in the log-log plane.

To evaluate the functional relationships between the variables we have used a linear regression analysis. However, this method does not give a unique result, because the choice of the dependent and independent variables is not obvious (a detailed discussion of the linear regression problem is given in the

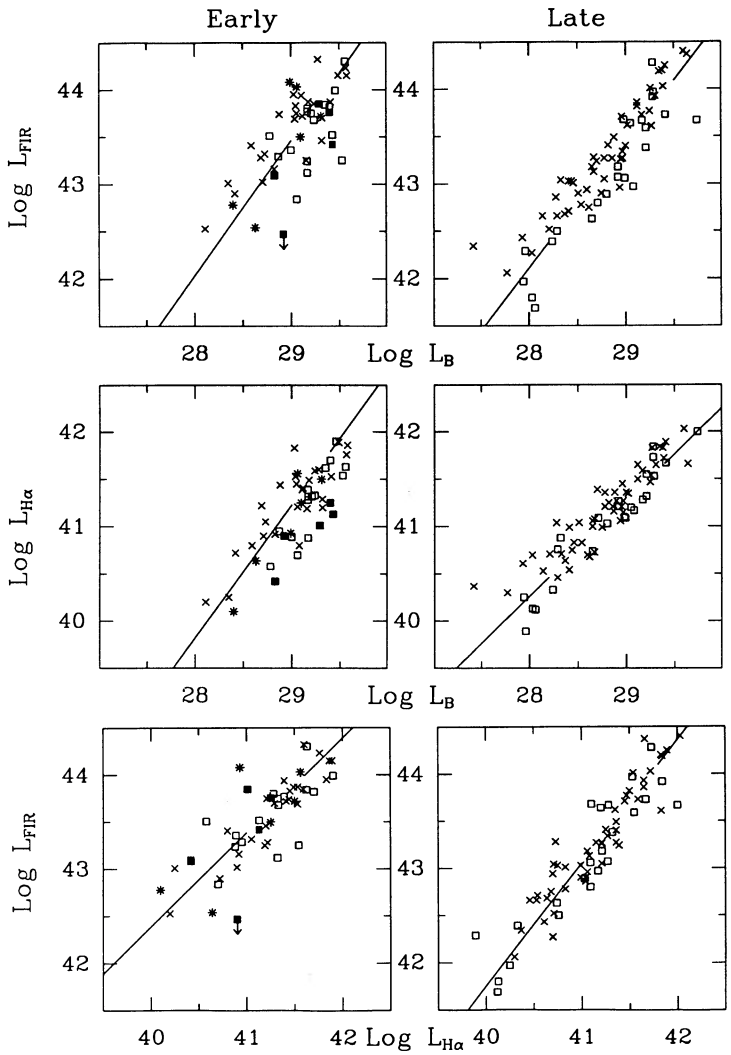

FIG. 1.—The luminosity-luminosity plots for the two subsamples of early- (*left panels*) and late- (*right panels*) type spirals. Galaxies with $D_{25} > 4'$ are indicated with an open box. Filled boxes and asterisks (*) indicate galaxies with evidence of nuclear emission (from Kennicutt and Kent 1983) for large and small diameter galaxies, respectively. The best-fit regression line from Table 3 appropriate to each subsample is also shown.

TABLE 2

LINEAR REGRESSION RESULTS: $y = A + Bx$

		EARLY-TYPE SAMPLE			LATE-TYPE SAMPLE		
y	x	r_c	A	B	r_c	A	B
$\log L_{FIR}$	$\log l_B$	0.73 (0.83)	5.88	0.95 ± 0.13 (1.09 ± 0.13)	0.99 (0.94)	9.68	1.16 ± 0.07 (1.13 ± 0.06)
$\log l_B$	$\log L_{FIR}$		4.61	0.56 ± 0.08		−1.52	0.70 ± 0.04
$\log L_{H\alpha}$	$\log l_B$	0.80 (0.86)	10.54	1.05 ± 0.11 (1.13 ± 0.12)	0.92 (0.92)	14.56	0.92 ± 0.05 (0.86 ± 0.05)
$\log l_B$	$\log L_{H\alpha}$		4.00	0.60 ± 0.06		−9.05	0.92 ± 0.05
$\log L_{FIR}$	$\log L_{H\alpha}$	0.81 (0.85)	10.04	0.81 ± 0.08 (0.85 ± 0.09)	0.92 (0.93)	−5.45	1.18 ± 0.06 (1.20 ± 0.07)
$\log L_{H\alpha}$	$\log L_{FIR}$		5.81	0.81 ± 0.08		9.96	0.72 ± 0.04

NOTE.—The numbers in parentheses refer to the sample of small galaxies ($D_{25} \leq 4'$).

Appendix). To overcome this problem, we have first calculated regressions for both the direct and the inverse relation between each pair. In this way we obtain two slopes, listed in Table 2, which represent the two limits of the "true" slope of the underlying relationship. To obtain a more direct estimate of the slope and its uncertainty, we have also applied a revised regression analysis (see the Appendix), which minimizes the Cartesian distances between the points and the regression line, rather than the distances along the y axis. In the assumption that the errors in the x and y axes are comparable, we obtain the results presented in Table 3. Since we only have one upper limit in the far-infrared (in the early-type sample), we have resolved to disregard that one galaxy to ease the analysis.

Since only a few galaxies of large angular size have accurate far-infrared flux measurements, we have redone the analysis on two subsamples containing only galaxies with 25th mag isophotal diameters smaller than $\sim 4'$, to ensure that a possible bias introduced by the small *IRAS* beam size did not affect our results (see, e.g., FGT). The early sample is thus reduced to 32 objects, the late sample to 51. The correlations for the "small" samples are tighter (cf. Fig. 1), but the resulting parameters are entirely consistent with those of the corresponding samples of all size galaxies (cf. Tables 2 and 3).

We also checked whether the exclusion of the objects not detected in Hα in the Kennicutt and Kent survey could bias our results. Only one object was excluded from the "late" sample, and therefore these results are not affected. However, $\sim \frac{1}{3}$ of the "early" sample galaxies were not detected in Hα, and the sample that we are using is therefore selected for "Hα bright" galaxies. We have estimated upper limits to the Hα luminosity of these galaxies, using the typical errors on the Hα equivalent widths (W_λ) quoted by Kennicutt and Kent (1983). These were converted to errors on the fluxes, by scaling for the optical magnitude of the galaxies and using a conversion factor estimated from the detected galaxies. We found that the distribution of these upper limits is consistent with that of the detections in the luminosity-luminosity plots of Figure 1. This gives us confidence that the exclusion of these galaxies does not affect severely our results for the "early" sample.

The formal results of the analysis (Tables 2 and 3) clearly show the following.

1. *All pairs of variables are highly correlated.* These correlations are not introduced by a Malmquist bias, since correlations are observed also in the corresponding plots for the fluxes and for the surface brightness relative to the optical size, which compares distance-independent quantities (not shown here; see PH). Both the correlation coefficients and the best-fit slopes are consistent with the corresponding values for the luminosity correlations.

2. *The slopes of some correlations deviate from linearity.* For the late sample in particular, the only linear relationship is the one between l_B and $L_{H\alpha}$. The other two relationships indicate a similar increasing fraction of L_{FIR} relative to $L_{H\alpha}$ and l_B with increasing luminosities. We have further checked this point by also looking at the plots of the flux ratios. We find that the only strong correlation is that between FIR/Hα versus FIR/B (see below), which we show in Figure 2.

3. *The slopes of the $L_{H\alpha} - L_{FIR}$ and $L_{H\alpha}$–l_B correlations are different in the early- and late-type samples.* These differences are confirmed by the different distributions of the residuals of the early- and late-type samples about the mean regression line of the entire sample. Similarly, different distributions of residuals are obtained for the two subsamples, when best-fit regression line of either one is used for comparison. A Kolmogoroff-Smirnoff (KS) test applied to the comparison of the distribution of the residuals for the early- and late-type samples about the same regression line indicates that, in all cases, the best fit from the early (late) sample cannot fit the data for the late (early) sample, as shown by Table 4.

4. *The correlations present more scatter in the early-type*

TABLE 3

LINEAR REGRESSION RESULTS: $y = A + Bx$
(minimizing the orthogonal distances)

		EARLY-TYPE SAMPLE			LATE-TYPE SAMPLE			TOTAL SAMPLE		
y	x	r_c	A	B	r_c	A	B	r_c	A	B
$\log L_{FIR}$	$\log l_B$	0.75	2.05	1.43 ± 0.21	0.91	5.15	1.32 ± 0.08	0.88	4.80	1.33 ± 0.07
		(0.84)	(3.40)	(1.39 ± 0.18)	(0.94)	(8.30)	(1.22 ± 0.07)	(0.92)	(6.85)	(1.27 ± 0.07)
$\log L_{H\alpha}$	$\log l_B$	0.82	0.34	1.41 ± 0.16	0.92	12.26	1.00 ± 0.05	0.85	11.10	1.03 ± 0.06
		(0.87)	(1.14)	(1.38 ± 0.16)	(0.92)	(14.54)	(0.92 ± 0.06)	(0.87)	(11.67)	(1.02 ± 0.07)
$\log L_{FIR}$	$\log L_{H\alpha}$	0.81	2.39	1.00 ± 0.11	0.93	−10.45	1.31 ± 0.07	0.87	−9.44	1.28 ± 0.07
		(0.85)	(2.20)	(1.00 ± 0.12)	(0.94)	(−10.80)	(1.31 ± 0.08)	(0.88)	(−8.27)	(1.26 ± 0.08)

NOTE.—The numbers in parentheses refer to the sample of small galaxies ($D_{25} \leq 4'$).

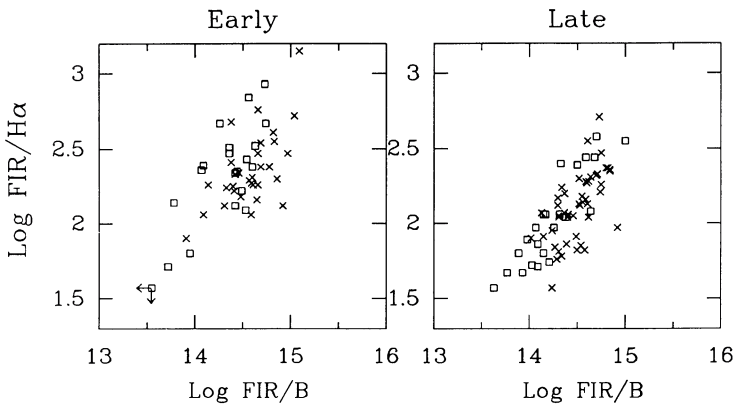

FIG. 2.—Plot of the ratios FIR/*B* vs. FIR/Hα for early- (*left*) and late- (*right*) spirals. Open boxes identify large diameter galaxies.

sample than in the late-type sample. The correlation coefficients of the early-type sample are systematically smaller for a smaller number of objects, which is a sign of a lower degree of correlation.

We have also tested the significance of the correlations with the nonparametric Spearman rank test, which allows us to evaluate the strength of a given correlation, without having to rely on the assumption of a specific functional dependence between the variables (see also FGT). The results obtained with the nonparametric analysis are entirely consistent with those from the regression analysis and indicate in general a higher degree of correlation in later type galaxies.

b) Comparison with Previous Work

The existence of correlations between Hα, *B*, and/or FIR has already been reported (Kennicutt and Kent 1983; Gavazzi, Cocito, and Vettolani 1986; Moorwood, Veron-Cetty, and Glass 1986; PH; FGT). Our results are in general agreement with these earlier reports, although these papers typically considered only two of the three variables at a time and did not address directly the issue of all the functional dependencies between the variables. In particular, Kennicutt and Kent found a larger spread in the distribution of the Hα/*B* ratios of early-type spirals than in that of late-type spirals, which is clearly a consequence of the nonlinear versus linear slopes found for the two samples (see Tables 2 and 3). Gavazzi, Cocito, and Vettolani (1986) suggested that the functional relations between optical and far-infrared luminosity depend on morphology, contrary to our results. However, this conclusion was based on the presence of the two "extreme" classes, the S0a's and the Irregulars (see their Fig. 1), which are not well sampled here.

Hα, *B*, and FIR, together with other related quantities, have been considered in the work of PH, which is based on a smaller sample of spirals mostly contained in the present sample and inclusive of all morphological types at the same time. To compare our results with theirs, we have extended our correlation analysis to include the flux ratios FIR/Hα, FIR/*B*, and Hα/*B*; the far-infrared color 60/100 (derived from the far-infrared fluxes listed in the *IRAS* catalog); the optical colors $(B-V)$ and $(U-B)$ (from de Vaucouleurs, de Vaucouleurs, and Corwin 1976); and the Hα equivalent width W_λ(Hα) (from Kennicutt and Kent 1983), although this quantity is closely related to the ratio Hα/*B*. We have evaluated the significance of the correlations with the Spearman rank test. Table 5 summarizes some of our results, to which we will refer below. As for the regression analysis, we have always checked that the subsamples of small diameter galaxies yielded consistent results.

Our results only partially agree with those of PH. We find that the most significant correlation is the FIR/*B*–FIR/Hα in the late-type sample (Figure 2), followed by FIR/*B*–FIR and FIR/Hα-FIR, shown in Fig. 3. With only three exceptions, namely FIR/*B*–60/100, FIR/*B*–Hα/*B*, and FIR/*B*–FIR, we find no one-to-one correspondence between the significance of a given correlation in the late- and early-type spiral samples. The results of Table 5 confirm the finding of the regression analysis, that there is a similar excess far-infrared emission compared to both Hα and *B* luminosities in the more luminous late-type spirals. Moreover, the results of Table 5 indicate a higher 60/100 flux ratio for galaxies with larger far-infrared excess (which on average are the more luminous galaxies), indicating a higher average temperature in these objects (see also deJong 1986). To a lesser degree, there is also an indication that warmer dust is found associated with other indications of star-formation activity (bluer $U-B$ colors, larger Hα equivalent widths) in late-type galaxies.

The links between FIR/Hα (IRE in PH) with 60/100, W_λ(Hα), and $(B-V)$, discussed by PH, have instead low significance, which increases when all morphological types are analyzed

TABLE 4

K-S TEST RESULTS[a]

	Hα-FIR			FIR-B			Hα-B		
BEST FIT FOR:	D_{max}	χ_2^2	P	D_{max}	χ_2^2	P	D_{max}	χ_2^2	P
Early	0.40	19.0	8×10^{-5}	0.26	8.0	0.02	0.50	29.7	1×10^{-5}
Late	0.39	18.0	1×10^{-4}	0.12	1.7	0.40	0.39	18.0	1×10^{-4}
Total	0.41	20.0	5×10^{-5}	0.11	1.4	0.50	0.27	9.0	1×10^{-2}

[a] K-S test on the comparison between the distribution of residuals of the early- and late-type samples about the best-fit regression lines of the early-, late-, and total type samples.

TABLE 5

SPEARMAN RANK TEST PROBABILITIES

CORRELATIONS		EARLY-TYPE SAMPLE			LATE-TYPE SAMPLE			TOTAL SAMPLE		
		N	t	Prob	N	t	Prob	N	t	Prob
FIR/Hα	FIR/B	50	3.7	5×10^{-4}	71	9.4	$\ll 5 \times 10^{-7}$	121	9.1	$<5 \times 10^{-7}$
FIR/Hα	60/100	50	2.2	0.03	71	1.7	...	121	3.2	2×10^{-3}
FIR/Hα	W_λ	50	−1.0	...	71	−0.6	...	121	−3.4	10^{-3}
FIR/Hα	FIR	50	2.1	0.03	71	7.1	$<5 \times 10^{-7}$	121	8.4	$<5 \times 10^{-7}$
FIR/Hα	($B-V$)	41	1.3	...	59	3.6	5×10^{-4}	100	6.0	$<5 \times 10^{-7}$
FIR/B	Hα/B	50	4.8	10^{-5}	71	4.1	10^{-4}	121	4.8	5×10^{-6}
FIR/B	($B-V$)	41	−4.6	5×10^{-5}	59	1.6	...	100	−0.4	...
FIR/B	($U-B$)	29	−3.1	5×10^{-3}	34	0.9	...	63	−0.6	...
FIR/B	60/100	50	4.9	10^{-5}	71	4.9	10^{-5}	121	7.2	$<5 \times 10^{-7}$
FIR/B	FIR	50	6.1	$<5 \times 10^{-7}$	71	7.3	$<5 \times 10^{-7}$	121	10.1	$<5 \times 10^{-7}$
($U-B$)	60/100	29	−2.6	.01	34	−5.0	10^{-5}	63	−2.8	0.03
60/100	W_λ	50	1.9	...	71	5.1	5×10^{-6}	121	3.3	10^{-3}

NOTE.—N is the number of objects in each sample. The parameter t is distributed according to the Student's t-distribution with $(N-2)$ degrees of freedom.

together. Moreover, contrary to PH, we obtain positive Spearman rank coefficients for the FIR/Hα–60/100 and FIR/Hα–($B-V$) pairs. The different selection criteria used here and by PH can probably explain these discrepancies. In particular, PH have restricted their analysis only to galaxies with high-quality far-infrared and Hα data that are detected as point sources by *IRAS*. Although their sample should be statistically comparable to our small-size sample, the additional requirement of high-quality data (effectively a higher cut in flux) results in the exclusion of a few lower luminosity galaxies, which typically have cooler far-infrared colors, as a result of the existing correlation between the FIR/B and the 60/100 ratios (Table 5). Since these correlations are marginal, a difference of a few galaxies can turn very weak positive trends into the negative trends reported by PH.

IV. DISCUSSION

The correlations examined the previous section present a larger spread for the early-type spirals than for the later types and the best-fit parameters are different in the two samples. Similar morphological effects had been noticed by Kennicutt (1983), Kennicutt and Kent (1983), and FGT who linked them to the presence of dominant stellar bulges and possibly nuclear emission. Since bulges cannot be separated from the disk emission with the present data, we will not discuss early-type systems further. We will concentrate instead on disk-

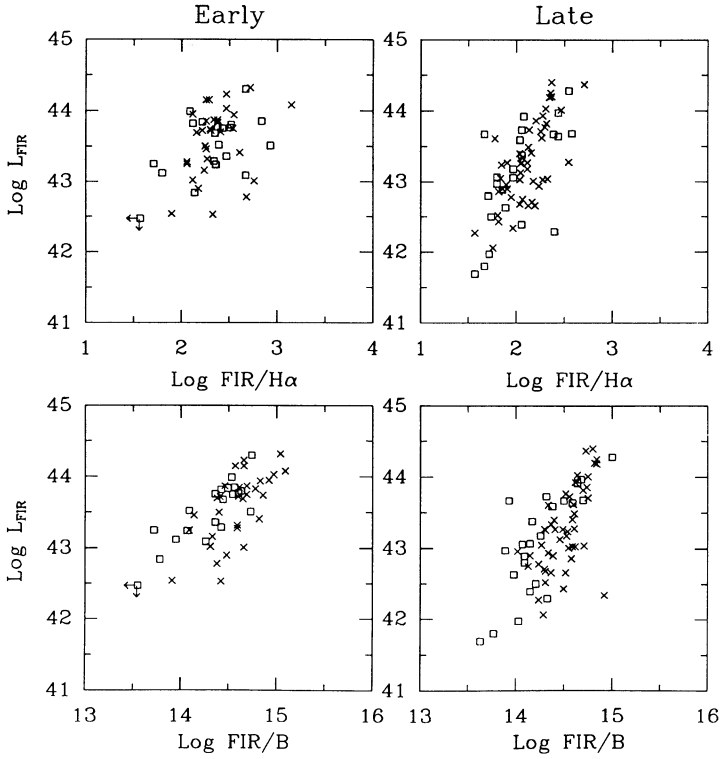

FIG. 3.—FIR luminosity plotted against the FIR/Hα (*top*) and FIR/B (*bottom*) ratios for early- (*left*) and late- (*right*) spirals. Open boxes identify large diameter galaxies.

dominated spirals, which present a more homogeneous, and therefore simpler to investigate, stellar population.

a) Highly Obscured Starburst Components in More Luminous Galaxies

In the previous section we have shown that there is a relative increase of the far-infrared emission with respect to Hα and *B* with galaxy luminosity, while there is a parallel increase of Hα with *B* (Tables 2 and 3; Fig. 1), and that galaxies with larger far-infrared excesses tend to have warmer far-infrared temperatures (Table 5; this last point was previously discussed by Soifer, Neugebauer, and Houck 1987; Helou 1987). The relative excess far-infrared over optical (*B*) emission in more luminous galaxies has been discussed by FGT, who suggested that this excess originates in obscured starburst regions and is therefore "warm." FGT's suggestion can explain our results if the optical depth of these regions is large enough to suppress both the *B* and Hα emission, which would also result from the star-formation activity. Present data on nuclear starburst regions show that extinction can indeed by very large (e.g., $A_V = 15$ and 25 in NGC 253 and M82, respectively; Wynn-Williams *et al.* 1979; Rieke *et al*, 1980). Dust-embedded OB stars have also been used by Buat and Deharveng (1988) to explain why their model underestimates the luminosity of the warm far-infrared component. With the present data we cannot comment on whether these regions are associated with the galaxy nucleus (as suggested by Rowan-Robinson and Crawford 1986) or are distributed in the disk. Imaging in the far-infrared is needed to definitely decide this issue.

b) Warmer and Cooler Far-Infrared Components

Recent studies suggest that the far-infrared emission in spiral galaxies results from the contribution of a warmer and a cooler component, that seem to be present in different percentages in galaxies with different properties (Cox, Krueger, and Mezger 1986; PH; Rowan-Robinson and Crawford 1986; de Jong 1986; FGT). As discussed in § IV*a*, the strongest statistical links point to an association of excess far-infrared emission with the warm far-infrared component. This is in apparent contrast with the conclusions of PH who suggest that the cooler component dominates in red galaxies with *large* infrared excesses and is due to the general stellar field, while the warmer component, linked to recent star formation, dominates in blue galaxies characterized by *low* FIR/Hα ratios, which on average are not the most luminous ones. Moreover, the presence of correlations between the far-infrared 60/100 ratio and indicators of star-formation activity ($U-B$, W_λ; cf. Table 5) is also clear from our analysis. These results suggest that two possibly independent effects determine the incidence of the warm far-infrared emission in disk galaxies. The principal one is a luminosity effect, resulting in a dominant warm FIR component in galaxies with, on average, *higher* FIR/Hα and FIR/*B* ratios, which also tend to be the most luminous (cf. good correlation between L_{FIR} and FIR/*B*), and are not particularly blue (cf. no correlation between luminosity and $U-B$, see also FGT). The second effect is the presence of widespread intense star formation, as also pointed out by PH.

The dependence of the warm component on both luminosity and star-formation activity is well illustrated by Fig. 4, where the 60/100 color is plotted as a function of the far-infrared excess relative to the blue light. Fig. 4*a*, where different symbols have been used for galaxies in different luminosity ranges, shows clearly the luminosity effect: more luminous galaxies tend to have warmer far-infrared colors and larger far-infrared excesses. In Figure 4*b* instead, different symbols identify galaxies in different ranges of Hα equivalent widths. It is clear from this figure that galaxies with more intense star-formation activity tend also to have warmer far-infrared colors and larger far-infrared excesses. However, comparison of Figure 4*a* and 4*b* shows that the more luminous galaxies are not necessarily those with larger W_λ and vice versa. The presence of these two effects may account for the scatter in the correlation.

The association between warmer FIR colors and star-formation activity becomes more evident in samples of blue, irregular galaxies. The data by Gallagher and Hunter (1987) show in fact that these galaxies have warmer far-infrared colors

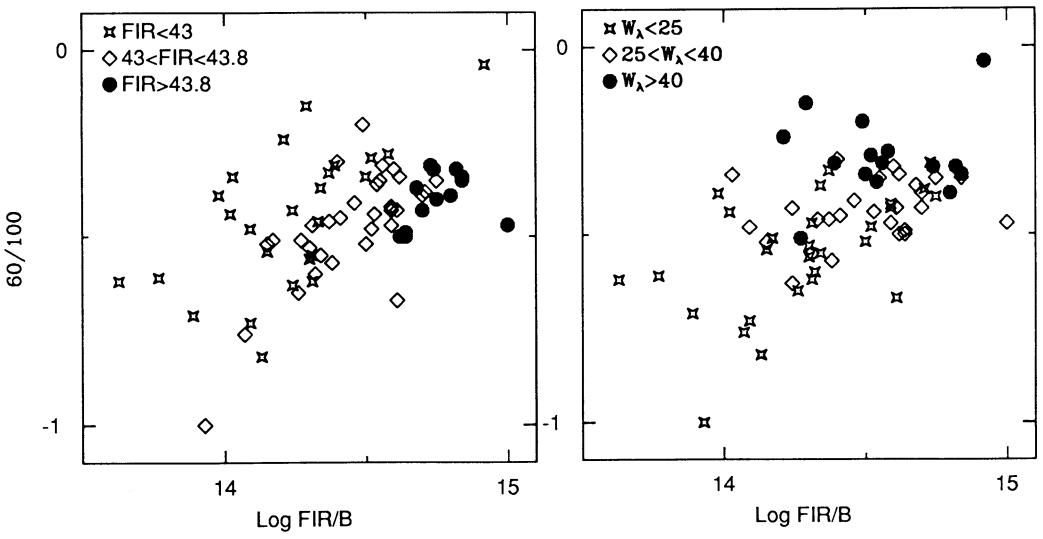

FIG. 4*a* FIG. 4*b*

FIG. 4.—Far-infrared colors (60/100 ratios) plotted against the far-infrared to blue ratios for the late-type spiral sample. (*a*) The different symbols identify galaxies in different ranges of far-infrared luminosity. (*b*) The different symbols identify galaxies in different ranges of Hα equivalent widths(W_λ).

than normal spirals, but similar FIR/B ratios, indicating probably different relative contributions of the two far-infrared components in spiral and more irregular blue systems. If the nonlinear FIR-B or FIR-Hα correlations that we observe in spirals are indeed due to the presence of a larger fraction of compact star-forming regions of large optical depths in luminous objects, the higher Hα/FIR ratios observed in blue star-forming galaxies can be eaily explained as due to the smaller optical depths characteristic of these systems (Gallagher and Hunter 1987) that allows a larger fraction of the Hα emission to escape.

c) Implications for the Initial Mass Function IMF)

The linear proportionality between Hα and B emission (Tables 2 and 3; Fig. 1) is evidence of a constant ratio of massive to intermediate/low mass stars in galactic disks, and therefore of a star-formation constant with galaxy luminosity and time over the last $\geq 10^9$ yr (Kennicutt and Kent 1983). This is apparently in conflict with other results, chiefly based on the nonlinear correlation observed between B and H (1.6 μm near-infrared) in spiral galaxies (see review in FGT), which suggest instead that the stellar population and star-formation history in disk-dominated galaxies are related to the total luminosity of the galaxy. This apparent contradiction, however, can be resolved if the IMF follows different power laws in different mass ranges (see Scalo 1986), with two additional constraints: the more massive portion of the IMF ($M \gtrsim$ 1–2 $M_\odot$) should not vary significantly from galaxy to galaxy; and the slope of the less massive portion should be a function of galaxy luminosity. The alternative of a bimodal IMF (Larson 1986), with the strength of the lower mass component only varying with galaxy luminosity would effectively mimic the same picture.

The constraint of an invariant stellar mass function for intermediate- to high-mass stars rules out the hypothesis that the far-infrared excess could be due to a larger fraction of heating sources in the disk population. This constraint is also consistent with our previous conclusion (§ IV*a*) that the far-infrared excess originates in compact starburst regions. It should be noted that red supergiants will also be formed in these regions as a result of the star-formation activity, and they will give an additional contribution to the H band emission (see discussion in FGT). If their emission is large enough to entirely explain the excess H band luminosity with respect to B, the stellar mass function could be invariant for all stellar masses.

V. CONCLUSIONS

Our analysis has shown that the Hα/FIR/B correlations in spiral galaxies depend upon the morphological types of the galaxies, most likely as a result of the presence of a bulge component in early-type spirals. Since we cannot separate the bulge contribution from the total emission with the present data, we have confined our analysis to a sample of late-type spirals to investigate the properties of spiral disks.

To explain the lack of both Hα and B relative to FIR in these galaxies, we need an additional source of far-infrared emission in the more luminous spirals, in agreement with the results of FGT. This can be obtained if compact starburst regions, with large intrinsic absorption, are preferentially found in more luminous systems. This additional FIR component would also explain the larger 60/100 colors observed in the more luminous spiral galaxies (deJong 1986; Helou 1987). However, we also find evidence of an independent link between warmer far-infrared colors and optical indicators of starburst activity, which is mostly evident in the comparison with blue irregular galaxies of small optical depth.

Our data are consistent with a constant star-formation rate in galactic disks over the last few billion years (see Kennicutt 1983). However, to explain some of the FGT results, we suggest that there is a break in the stellar mass function at $M \sim 1\ M_\odot$ and that the relative number of stars with masses smaller than the break value is a function of total galaxy luminosity. This requirement could be relaxed if a significant fraction of the near-infrared emission is due to a population of red supergiants, which could be present in the starburst regions discussed above and could account for the relative excess H band luminosity in more luminous spirals.

G. F. acknowledges useful discussions with other participants in the Aspen Workshop on Galaxies (1987 June), in particular with J. Gallagher and R. Larson, and thanks the Arcetri Observatory for hospitality. We also thank the anonymous referee who suggested several improvements to the paper. We acknowledge the financial support of the Italian Piano Spaziale Nazionale and NASA contract NAS8-30751 and (JPL) 958021.

APPENDIX

LINEAR REGRESSION BETWEEN RANDOM VARIABLES

Linear regression analysis provides a statistical tool to estimate the relationship among two or more variables, one of which (y) is assumed to depend linearly upon the others $[x_{(\alpha)}]$, with a linear relation of the kind: $y = a + \sum_\alpha b_{(\alpha)} x_{(\alpha)}$. The usual assumption is that only the dependent variable is affected by measurement errors: consequently the best-fit coefficients $[a, b_{(\alpha)}]$ are obtained by minimizing the dispersion of the measured points (y_i) around the predicted position $\{y[x_{(\alpha)i}]\}$. In many cases of interest, however, one has to draw a relationship between variables with comparable intrinsic dispersions. In these cases the standard linear regression analysis fails, because one cannot decide unambiguously which variable should be considered as the dependent one; on the other hand, the results depend upon the choice. In the following we shall present a generalization of linear regression to the case in which all variables are affected by an error. For the sake of simplicity only the two-dimensional case ($y = a + bx$) will be considered here.

The problem of linear regression between two random variables has been discussed to some extent by Kendall and Stuart (1976), who have also derived the equations for the coefficients of the best-fit line; we shall recall these relations and in addition we shall also derive the equations to estimate the errors on the coefficients. As Kendall and Stuart pointed out, a linear regression between two random variables can be performed only when their statistics are known, otherwise the solution is not unique. In the latter case

the solution can be parametrized in terms of the ratio between the intrinsic dispersions of the two variables (as will be done in this paper); alternatively, if more than two variables are treated at the same time, the needed information on the error statistics can be extracted from the data themselves (R. Bandiera, in preparation).

In the generalization of linear regression presented below, we shall assume that the two variables are affected by Gaussian errors, with standard deviations σ_x and σ_y, respectively, and furthermore, that the probability distributions of the errors do not vary from point to point. Except for the fact that we allow finite dispersion along both axes, these assumptions coincide with those of the standard linear regession.

To find the best-fit line one should minimize the sum of the square Euclidean distances of data points from the line itself, using σ_x and σ_y as units along the x and y axis, respectively. The distance d of a point (x_i, y_i) from the line is

$$d = |a + bx_i - y_i|/\sigma_y\sqrt{(1 + R^2b^2)}\,, \tag{A1}$$

where $R = \sigma_x/\sigma_y$ ($R = 0$ is used in standard linear regression). Therefore one can define a functional F as the sum of the squared distances, multiplied by a factor $\sigma_y{}^2$, i.e.,

$$F = \sum_i (a + bx_i - y_i)^2/(1 + R^2b^2)\,. \tag{A2}$$

The best-fit value of the intercept a can be readily obtained by minimizing equation (A2): $a = (\sum_i y_i - b\sum_i x_i)/N$, where N is the number of data points. Substituting into equation (A2) we obtain

$$F = (b^2S_{xx} - 2bS_{xy} + S_{yy})/(1 + R^2b^2)\,, \tag{A3}$$

where $S_{xx} = \sum_i x_i{}^2 - \sum_i x_i \sum_k x_k/N$, $S_{xy} = \sum_i x_i y_i - \sum_i x_i \sum_k y_k/N$, and $S_{yy} = \sum_i y_i{}^2 - \sum_i y_i \sum_k y_k/N$.
For convenience, let

$$\begin{aligned} Q &= (S_{xx} - R^2S_{yy})/2RS_{xy}\,, \\ P &= \text{sign}\,(S_{xy})\sqrt{1 + Q^2} = \sqrt{(S_{xx} + R^2S_{yy})^2 - 4R^2(S_{xx}S_{yy} - S_{xy}{}^2)}/2RS_{xy}\,. \end{aligned} \tag{A4}$$

The functional F reaches an extremum when $B^2 + 2QB - 1 = 0$, where $B = Rb$. Solutions of this equation are $B_\pm = -(Q \pm P)$. Alternatively, we can write the above quantities Q and P as $Q = (1 - B_\pm{}^2)/2B_\pm$ and $P = \mp(1 + B_\pm{}^2)/2B_\pm$. At $B = B_\pm$ the value of the functional is

$$\begin{aligned} F_\pm &= \frac{(S_{yy} - B_\pm{}^2 S_{xx}/R^2)}{(1 - B_\pm{}^2)} = \left[(S_{xx} + R^2S_{yy}) - \frac{1 + B_\pm{}^2}{1 - B_\pm{}^2}(S_{xx} - R^2S_{yy})\right]\Big/2R^2 \\ &= \frac{[(S_{xx} + R^2S_{yy}) \pm \sqrt{(S_{xx} + R^2S_{yy})^2 - 4R^2(S_{xx}S_{yy} - S_{xy}{}^2)}]}{2R^2}\,. \end{aligned} \tag{A5}$$

The absolute minimum of the functional is F_-; therefore the slope of the best-fit line is $b_- = B_-/R$.

The uncertainty on the best-fit slope can be evaluated in terms of the dispersion Δx_i and Δy_i. From the functional dependence of b on Q (hereafter the symbols b and F will be used instead of b_- and F_-) we derive $\Delta b = |b/P|\Delta Q$. Q is also a simple function of S_{xx},

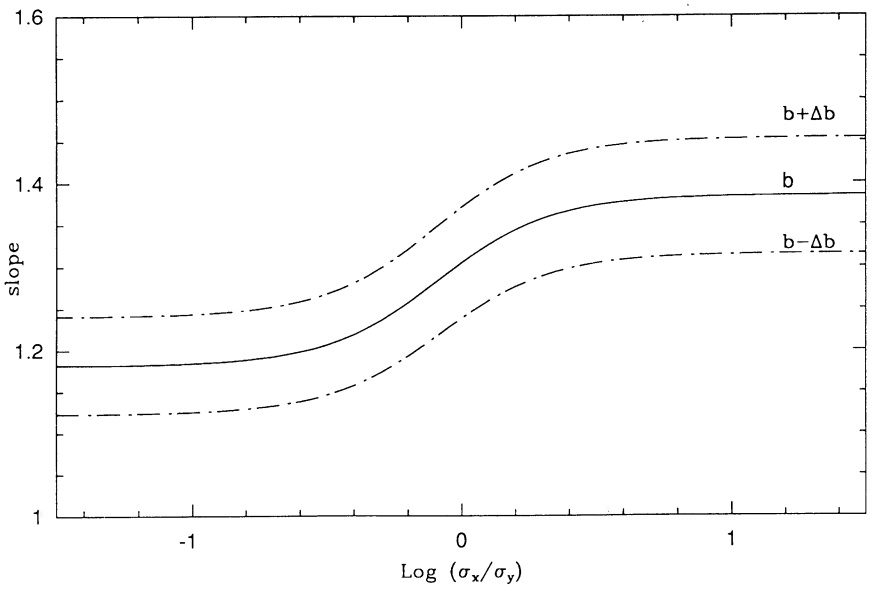

FIG. 5.—The dependence of the slope b (*solid line*) and its estimated error (*dot-dashed lines*) as a function of the relative dispersion on the x and y axes (see text). $\sigma_x/\sigma_y = 0$ corresponds to the standard linear regression analysis (cf. Table 2).

S_{xy}, and S_{yy}; thus ΔQ can be determined as follows:

$$\Delta Q = \sqrt{\sum_i \left[\left(\frac{\partial Q}{\partial S_{xx}} \frac{dS_{xx}}{dx_i} + \frac{\partial Q}{\partial S_{xy}} \frac{dS_{xy}}{dx_i} \right)^2 (\Delta x_i)^2 + \left(\frac{\partial Q}{\partial S_{yy}} \frac{dS_{yy}}{dy_i} + \frac{\partial Q}{\partial S_{xy}} \frac{dS_{xy}}{dy_i} \right)^2 (\Delta y_i)^2 \right]}$$

$$= \frac{\sqrt{(S_{xx} - 2RQS_{xy} + R^2Q^2S_{yy})\sigma_x{}^2/R^2 + (R^2S_{yy} + 2RQS_{xy} + Q^2S_{xx})\sigma_y{}^2}}{|S_{xy}|}, \quad \text{(A6)}$$

where we have used the fact that each $\Delta x_i = \sigma_x$ and each $\Delta y_i = \sigma_y$. From the definition of F in equation (A2), $\sigma_y{}^2$ can be written as $\sigma_y{}^2 = F/(N-2)$. Therefore, the error on the slope can be estimated from

$$\Delta b = |b/S_{xy}| \sqrt{(S_{xx} + R^2S_{yy})F/(N-2)}\,. \quad \text{(A7)}$$

For $R = 0$, Δb reduces to the values obtained from the standard regression analysis. Figure 5 shows an example of the dependence of b and Δb from the relative dispersions on the x and y axes, for the Hα – FIR correlation of the late-type spirals.

The error on the intercept is instead

$$\Delta a = \sqrt{(1 + R^2b^2)F/N(N-2) + \left(\sum_i x_i/N \right)^2 (\Delta b)^2}\,. \quad \text{(A8)}$$

It consists of two parts: the first term indicates the uncertainty in determination of the intercept due to the thickness of the strip of data points, while the second one indicates the effect of variations in the slope of the fitting line on the intercept.

REFERENCES

Buat, V., and Deharveng, J. M. 1988, *Astr. Ap.*, **195**, 60.
Cataloged Galaxies and Quasars Observed in the IRAS Survey 1985, prepared by C. J. Lonsdale, G. Helou, J. C. Good, and W. Rice (Pasadena: Jet Propulsion Laboratory).
Cox, P., Krueger, E., and Mezger, P. G. 1986, *Astr. Ap.*, **155**, 380.
de Jong, T. 1986, in *Spectral Evolution of Galaxies*, ed. C. Chiosi and A. Renzini (Dordrecht: Reidel), p. 111.
de Vaucouleurs, G., de Vaucouleurs, A., and Corwin, H. G. 1976, *Second Reference Catalogue of Bright Galaxies* (Austin: University of Texas Press).
Fabbiano, G., Gioia, I. M., and Trinchieri, G. 1988, *Ap. J.*, **324**, 749 (FGT).
Gallagher, J. S., III, and Hunter, D. A. 1987, in *Star Formation in Galaxies*, ed. C. J. Lonsdale Persson (NASA Conference Publication 2466), p. 167.
Gavazzi, G., Cocito, A., and Vettolani, P. 1986, *Ap. J. (Letters)*, **305**, L15.
Helou, G. 1987, *Ap. J. (Letters)*, **311**, L33.
Kendall, M., and Stuart, A. 1976, *Advanced Theory of Statistics* (London: Charles Griffin), London.
Kennicutt, R. 1983, *Ap. J.*, **272**, 54.
Kennicutt, R. C., and Kent, S. M. 1983, *A.J.*, **88**, 1094.
Larson, R. B. 1986, *M.N.R.A.S.*, **218**, 409.
Moorwood, A. F. M., Veron-Cetty, M. P., and Glass, I. S. 1986, *Astr. Ap.*, **160**, 39.
Persson, C. J., and Helou, G. 1987, *Ap. J.*, **314**, 513 (PH).
Rice, W., *et al.* 1988, preprint.
Rieke, G. H., Lebofsky, M. J., Thompson, R. I., Low, F. J., and Tokunaga, A. T. 1980, *Ap. J.*, **238**, 24.
Rowan-Robinson, M., and Crawford, J. 1986, preprint.
Salpeter, E. E. 1955, *Ap. J.*, **121**, 161.
Sandage, A., and Tamman, G. A. 1981, *A Revised Shapley-Ames Catalog of Bright Galaxies*, (Washington, DC: Carnegie Institution of Washington).
Scalo, J. M. 1986, *Fund. Cosmic Phys.*, **11**, 1.
Soifer, B. T., Neugebauer, G., and Houck, J. R. 1987, *Ann. Rev. Astr. Ap.*, **25**, 187.
Tully, R. B., Mould, J. R., and Aaronson, M. 1982, *Ap. J.*, **257**, 527.
Wynn-Williams, C. G., Becklin, E. E., Matthews, K., and Neugebauer, G. 1979, *M.N.R.A.S.*, **189**, 163.

R. BANDIERA and G. TRINCHIERI: Osservatorio Astrofisico di Arcetri, Largo E. Fermi 5, 50125 Firenze, Italy

G. FABBIANO: Center for Astrophysics, 60 Garden Street, Cambridge, MA 02138